Catalyst Self-Assembly for Scalable Patterning of Sub 10 nm Ultrahigh Aspect Ratio Nanopores in Silicon

Citation: Smith, Brendan D. et al. "Catalyst Self-Assembly for Scalable Patterning of Sub 10 nm Ultrahigh Aspect Ratio Nanopores in Silicon." ACS Applied Materials & Interfaces 8, 12 (March 2016): 8043–8049 © 2016 American Chemical Society

As Published: http://dx.doi.org/10.1021/ACSAMI.6B01927

Publisher: American Chemical Society (ACS)

Persistent URL: http://hdl.handle.net/1721.1/111825

Version: Author's final manuscript: final author's manuscript post peer review, without publisher's formatting or copy editing

ACS APPLIED MATERIALS & INTERFACES

Research Article

www.acsami.org

Catalyst Self-Assembly for Scalable Patterning of Sub 10 nm Ultrahigh Aspect Ratio Nanopores in Silicon

Brendan D. Smith,[†] Jatin J. Patil,[†,‡] Nicola Ferralis,[†] and Jeffrey C. Grossman*[,†]

[†]Department of Materials Science and Engineering, Massachusetts Institute of Technology, 77 Massachusetts Avenue, Cambridge, Massachusetts 02139, United States

[‡]Department of Chemical Engineering, University of Waterloo, 200 University Avenue West, Waterloo, Ontario N2L 6G9, Canada

Supporting Information

ABSTRACT: Nanoporous silicon (NPSi) has received significant attention for its potential to contribute to a large number of applications, but has not yet been extensively implemented because of the inability of current state-of-the-art nanofabrication techniques to achieve sufficiently small pore size, high aspect ratio, and process scalability. In this work we describe the fabrication of NPSi via a modified metal-assisted chemical etching (MACE) process in which silica-shell gold nanoparticle (SiO_2−AuNP) monolayers self-assemble from solution onto a silicon substrate. Exposure to the MACE etchant solution results in the rapid consumption of the SiO_2 spacer shell, leaving well-spaced arrays of bare AuNPs on the substrate surface. Particles then begin to catalyze the etching of nanopore arrays without interruption, resulting in the formation of highly anisotropic individual pores. The excellent directionality of pore formation is thought to be promoted by the homogeneous interparticle spacing of the gold core nanocatalysts, which allow for even hole injection and subsequent etching along preferred crystallographic orientations. Electron microscopy and image analysis confirm the ability of the developed technique to produce micrometer-scale arrays of sub 10 nm nanopores with narrow size distributions and aspect ratios of over 100:1. By introducing a scalable process for obtaining high aspect ratio pores in a novel size regime, this work opens the door to implementation of NPSi in numerous devices and applications.

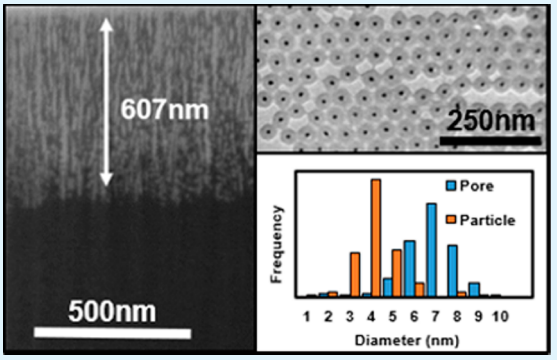

KEYWORDS: *nanoporous silicon, metal-assisted chemical etching, silica-shell gold nanoparticles, self-assembly, ultrahigh aspect ratio*

1. INTRODUCTION

Nanoporous silicon (NPSi) is a highly multifunctional material with a large number of current and potential applications. Although its fabrication via electrolytic etching was first discussed in 1956 by Uhlir,[1] NPSi has continued to receive significant attention, with modern advanced fabrication and characterization techniques revealing its utility to an ever-growing list of processes and devices. Recent work has highlighted the excellent potential of NPSi in applications including nanofiltration,[2−4] thermoelectrics,[5−10] lithium-ion battery anodes,[11−17] photovoltaics,[18−26] and catalysis.[27] Each of these applications stand to benefit from the integration of NPSi with decreased pore size, decreased interpore spacing, and increased pore aspect ratio, yet despite current advancements in nanofabrication technology, NPSi is nearing the limits of its accessible parameter space with regards to these three critical variables.

Current state-of-the-art electron beam lithography (EBL) coupled with deep reactive ion etching was recently demonstrated by Liu et al.[28] to be capable of fabricating nanobarrel structures with a wall thickness of 6.7 nm and aspect ratio of 50:1. Although potentially viable for the fabrication of specific components in nanoelectronics, EBL is limited by extremely high costs and processing times to device sizes of square micrometers and therefore not appropriate for any of the above-mentioned applications. Block copolymer lithography has received significant attention as a more scalable alternative and was utilized by Liu et al.[29] in conjunction with plasma etching to produce sub 10 nm features with aspect ratios of 17:1. Both techniques still require bombardment of the substrate with ions in a vacuum, however, meaning that they are intrinsically limited in their ability to be integrated into a high-throughput manufacturing process such as that required for the previously mentioned applications. The resulting implication is that new disruptive approaches capable of unprecedented resolution and morphology control will need to be implemented if the aforementioned applications are to benefit further from the integration of NPSi. In addition, these techniques must be scalable and high-throughput in order to facilitate the economically viable manufacturing of NPSi, while still achieving sub 10 nm pore sizes.

Received: February 15, 2016
Accepted: March 9, 2016

DOI: 10.1021/acsami.6b01927
ACS Appl. Mater. Interfaces XXXX, XXX, XXX−XXX

Such an approach is potentially available in metal-assisted chemical etching (MACE), an electrochemical technique that relies on noble metal-catalyzed anisotropic etching of nanopores in silicon (Si) and other semiconductor materials via a simple, scalable, and low-cost solution-based process.[30,31] The general reaction mechanism can be explained as follows for a gold catalyst deposited on the surface of a Si substrate and placed in an aqueous solution of hydrofluoric acid (HF) and hydrogen peroxide (H_2O_2). H_2O_2 is first reduced at the nanoparticle surface in what constitutes the cathode reaction.[31] The holes (h^+) generated in this reduction diffuse from the particle to the Si substrate, which is subsequently oxidized and dissolved by the HF at the anode.[32] The overall reaction also involves the reduction of protons (H^+) into hydrogen, which is released as gas (H_2).[33] As etching progresses, the gold nanoparticles maintain their proximity to the Si via van der Waals interactions,[34] thus continuing to catalyze the reaction.

MACE has recently been the focus of a large body of work in which noble metal patterns are implemented in the etching of positive features such as nanowires[13,35−41] and negative features including nanopores[21,27,30,34,42−49] in Si. Common methods of performing the latter are the deposition of colloidal nanoparticle catalysts on a Si surface,[44,45] deposition and dewetting of thin films,[16] or growth from solution.[19,20] Of these techniques, the deposition of presynthesized noble metal nanoparticles by drop-casting or similar methods affords the greatest degree of control over catalyst size, monodispersity, and position. Although this process is intrinsically low cost and very scalable, the etching mobility of nanoparticles along crystallographic orientations is far more difficult to control than interconnected lithographically defined, sputtered, or grown patterns with interfaces planar to the Si substrate. The result is the wandering of the particles laterally and partial loss of anisotropy, leading to significant variation in the pore depth and direction.[43,47] Causes of this phenomenon are thought to arise from multiple factors, including the nonspherical nature of the particles,[47] dislodging of the particles by the produced hydrogen gas,[47] and nonhomogenous injection of holes from the particles into the surrounding Si.[50] This challenge is compounded for very small nanoparticles because their shapes become dominated by faceting and no longer resemble spheres.[51] As a result, very little work has been carried out on the etching of pores in Si via MACE using sub 10 nm nanoparticle catalysts.

Here, we present an entirely solution-based, modified MACE process which has the ability to synthesize NPSi with sub 10 nm pore diameters, sub 10 nm interpore spacing, and pore aspect ratio of over 100:1. The developed method simultaneously allows for the fabrication of ordered nanopore arrays in a novel size regime, increases the etching homogeneity and anisotropy of nanoparticle catalyzed MACE, and drastically improves the scalability and high throughput nature of the process relative to conventional lithographic MACE approaches. The simple two-step process is carried out by first drop-casting silica-shell gold nanoparticles (SiO_2−AuNPs) onto a crystalline Si substrate. Solvent evaporation then facilitates SiO_2−AuNP self-assembly into close-packed monolayer arrays. Second, immersion of the SiO_2−AuNP monolayer coated Si into the MACE solution results in the rapid consumption of the silica shells by HF, leaving behind a well-spaced array of bare AuNPs on the surface. These AuNPs then seamlessly catalyze nanopore formation with an etching fidelity and consistency previously unobserved in the sub 10 nm regime. Through high-resolution transmission electron microscopy (TEM) and scanning electron microscopy (SEM), we characterize the deposited SiO_2−AuNP monolayers and arrays of nanopores pre- and post-MACE, respectively, allowing for the detailed monitoring of pore size, interpore spacing, and pore aspect ratio of the resulting NPSi. The developed technique opens new doors for the implementation of MACE to fabricate NPSi with sub 10 nm pore sizes over large areas in a scalable manner, which could help to facilitate the implementation of NPSi as a disruptive material in the previously discussed applications.

2. RESULTS AND DISCUSSION

2.1. Experimental Procedures. SiO_2−AuNPs (5 and 10 nm gold cores) are purchased from Sigma-Aldrich USA. Then, 5 nm particles are diluted 2× with H_2O, followed by a subsequent 5× dilution with acetone. The 10 nm particles are diluted 2× with acetone. Silicon wafers (Virginia Semiconductor Inc.) are boron-doped with resistivity 0.001−0.01 Ω·cm and thickness of 275 ± 25 μm. The prepared solutions are drop-cast onto a silicon wafer and allowed to dry in air. The coated substrate is then added to the MACE solution (5.65 M HF, 0.12 M H_2O_2) for varying times. The sample is removed and rinsed with DI water to stop the reaction. For imaging of pore cross sections, pores are filled with Al_2O_3 using atomic layer deposition (ALD, Cambridge NanoTech Savannah) for image contrast and conservation of the porous structure. Particle and pore sizes from SEM and TEM images were analyzed using ImageJ and MATLAB. Samples are imaged using a Zeiss Ultra Plus Field-Emission SEM, FEI Helios 660 Focused Ion Beam (for cross-sectional milling) with SEM (with attached EDAX Energy-Dispersive X-ray Spectroscopy [EDS] Detector), and a JEOL 2100 Transmission Electron Microscope.

2.1. Nanocatalyst Deposition. The use of noble-metal nanoparticles deposited from solution to catalyze the etching of nanopores via the MACE process in Si offers the benefit of being a scalable route of manufacturing NPSi. This method comes with its own set of challenges, however, primarily the control of the nanoparticle positioning on the surface, subsequently ensuring that the particle etches in a direction normal to the substrate surface during the process. The former is made difficult by the numerous complex forces that govern the behavior of the nanoparticles both in solution and in the self-assembly process during solvent evaporation. These include van der Waals, electrostatic, steric, solvation, depletion, capillary, convective, and friction forces.[52] The result of these interactions is that nanoparticles will often tend not to form monolayers of periodic spacing but instead exhibit a clustering behavior. Such a phenomenon is demonstrated in Figure 1A, which shows the aggregation of bare 50 nm AuNPs deposited via drop-casting from solution onto a crystalline Si wafer. This behavior is particularly detrimental to the etching of nanopores via the MACE process. Figure 1B shows an attempt at the etching of nanopores using a similarly aggregated group of bare 50 nm AuNPs, with the overall process shown via schematic in Figure 1C. The result of this attempt is the etching of relatively large, inhomogeneous pits in the Si (Figure 1C, Scheme 2), a morphology which is of little use to most relevant applications that require size-controlled individual pores. Other potentially undesirable results include the lateral etching of the nanocatalyst (Figure 1C, Scheme 3) or lack of etching altogether (Figure 1C, Scheme 4). AuNPs are understood to catalyze etching preferentially in the <100> direction but can also

DOI: 10.1021/acsami.6b01927
ACS Appl. Mater. Interfaces XXXX, XXX, XXX−XXX

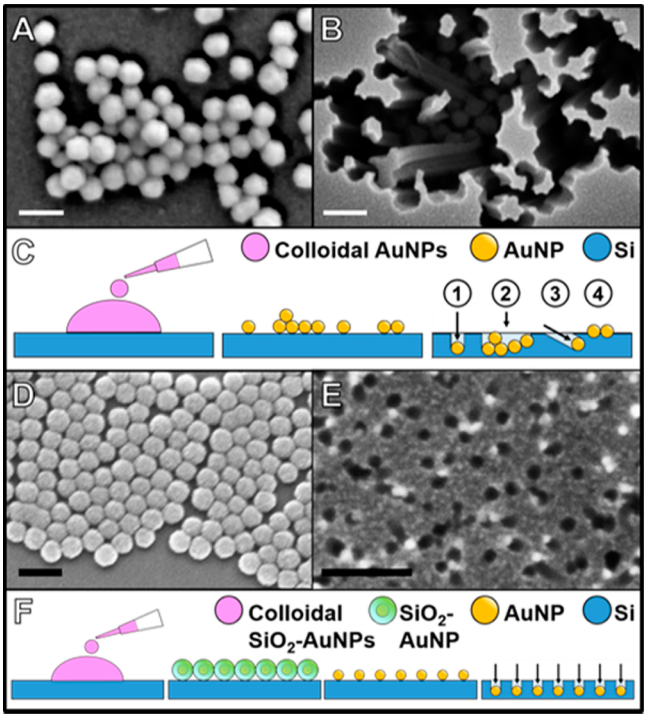

Figure 1. SEM images of crystalline Si substrate with drop-cast bare 50 nm AuNPs, (A) pre- and (B) post-MACE. (C) Process schematic of typical drop-casting of bare gold nanoparticles in the MACE process. Commonly observed phenomena include vertical etching (1), cluster etching (2), lateral etching (3), and disrupted etching (4). SEM images of crystalline Si substrate with drop-cast 10 nm core SiO_2–AuNPs, (D) pre- and (E) post-MACE. (F) Process schematic of the developed SiO_2–AuNP MACE process. Scale bars are 100 nm.

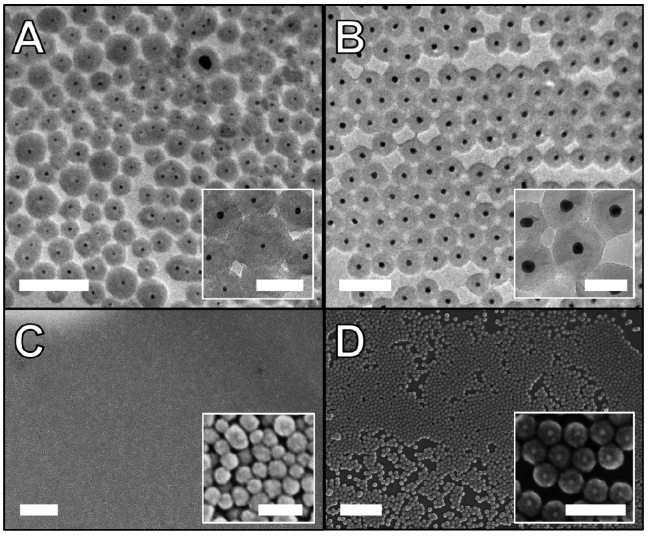

Figure 2. TEM images of (A) 5 nm and (B) 10 nm SiO_2–AuNPs drop-cast on a (100) Si membrane (scale bars are 100 nm, inset scale bars are 40 nm). SEM images of (C) 5 nm and (D) 10 nm SiO_2–AuNPs drop-cast on a (100) Si substrate (scale bars are 1 μm (C) and 500 nm (D); inset scale bars are 100 nm).

deviate from this path because of the nonhomogenous injection of holes from other surrounding catalysts[50] and their own facets[47] or to dislodgement by the hydrogen gas produced during etching.

We have addressed these challenges by developing a modified MACE process that involves the self-assembly of SiO_2–AuNPs monolayer arrays from solution on a crystalline Si substrate. The SiO_2 serves as a sacrificial spacer layer, which acts to maintain separation between the AuNP cores during deposition and self-assembly. Upon immersion into the MACE etchant, the SiO_2 shell is rapidly consumed, leaving behind periodically spaced AuNPs that begin the etching process. Figure 1D depicts a monolayer of SiO_2–AuNPs with 10 nm gold cores and SiO_2 shells of 15–20 nm thickness, whereas Figure 1E displays an etched Si substrate initially coated in a similar monolayer following 1 h of exposure to the MACE solution. Our overall process is demonstrated schematically in Figure 1F.

SiO_2–AuNPs can be synthesized in a simple solution chemistry process using tetraethylorthosilicate as a precursor with the ability to control shell thickness precisely ranging from 2 to 90 nm.[53,54] We focus here on the use of 5 and 10 nm diameter gold core SiO_2–AuNPs (SiO_2 shells thicknesses of 15–20 nm) in order to explore a new pore size regime in NPSi as well as to achieve a fine degree of pore size and interpore spacing control. Figure 2 displays TEM and SEM images of 5 and 10 nm SiO_2–AuNPs drop-cast from aqueous solutions of acetone and ultrapure water onto (100) Si wafers. Analysis by TEM (Figure 2A,B) shows both the outer SiO_2 shells and the well-spaced inner gold cores. Some regions of monolayer exhibit a well-ordered hexagonal close packed pattern, whereas others are slightly more spaced. Also observable are areas of sparse bilayer formation above the more closely packed monolayers (Figure 2A). The behavior of these partial bilayers during MACE will be discussed later in the context of porosity, interpore spacing, and process control. Figure 2C,D shows lower magnification SEM images of similar 5 and 10 nm SiO_2–AuNP arrays over multiple micrometers, elucidating the facile scalability of catalyst deposition. Though further exploration and optimization of different deposition techniques such as slope assembly[55] need to be carried out in order to achieve centimeter scale arrays of SiO_2–AuNP catalysts, there is no fundamental barrier to their realization.

2.3. Etching Characteristics. To demonstrate the time-based progression of the modified MACE process, drop-cast samples were exposed to the etchant solution for 15, 30, and 60 min (Figure 3). These images show progression of the MACE process after dissolution of SiO_2 shells. For both particle sizes, the SiO_2 shells should dissolve almost immediately after introduction to the MACE solution, leaving homogeneously spaced arrays of bare AuNPs. Many 5 nm core particles are observed to begin etching into the Si within 15 min (Figure 3A), whereas few 10 nm core particles demonstrate etching within the same time interval. After 60 min, most of the particles have etched into the Si and are no longer visible on the surface for both 5 and 10 nm samples. Even though ideally, all particles should etch into Si once their SiO_2 shells are dissolved, there are two possible reasons as to why this may not occur: (1) Once a particle's shell has etched, it may make contact with the Si surface either on a facet vertex or an edge of one of its crystal grains. Because the hole injection rate from a single particle is directly proportional to its contact surface area with the Si, its etching rate would be drastically lower than a particle with a planar interface between its facet and the Si surface. (2) Depending on the distribution of SiO_2 shell thicknesses of particles, some particles may start etching before their neighbors in close proximity, causing a small number of

DOI: 10.1021/acsami.6b01927
ACS Appl. Mater. Interfaces XXXX, XXX, XXX–XXX

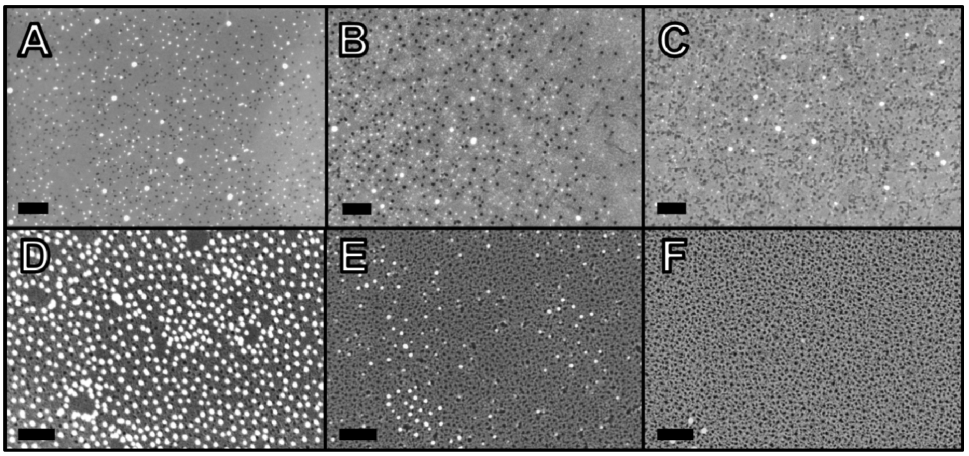

Figure 3. SEM images of drop-cast (A–C) 5 nm and (D–F) 10 nm SiO_2–AuNPs catalyzing MACE for (A and D) 15 min, (B and E) 30 min, and (C and F) 60 min. Scale bars are 100 nm.

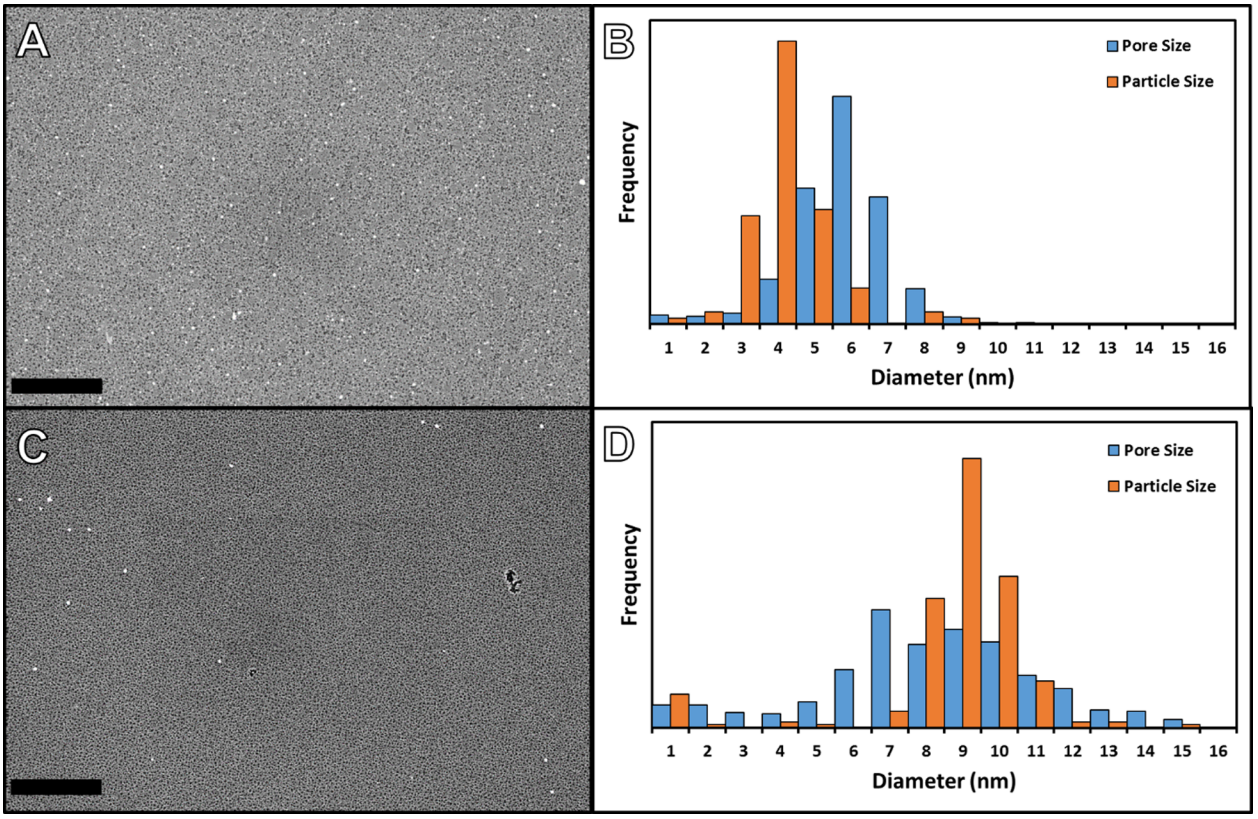

Figure 4. SEM images of NPSi produced via 60 min of modified MACE using drop-cast (A) 5 nm and (C) 10 nm SiO_2–AuNPs. Histograms of Au core (particle) and pore size distribution for the (B) 5 nm and (D) 10 nm SiO_2–AuNP MACE process. Scale bars are 500 nm.

particles to stay on the surface because of the lack of hole injection in the near vicinity from surrounding particles that have already penetrated the substrate.

Because directional etching is promoted by uniform hole injection into the Si, particles lacking adjacent neighboring particles are less likely to etch downward or at all. A promising observation is that little to no lateral or cluster etching has taken place after 60 min, possibly explained by the high degree of uniformity in hole injection from the closely spaced AuNPs, which seems to promote anisotropic etching in the <100> direction. As a result, we conclude that the quality of NPSi depends primarily on the quality and monodispersity of the SiO_2–AuNPs being MACE processed as well as the quality of the self-assembled monolayer produced.

2.4. NPSi Morphology. To elucidate quantitatively the morphology of the fabricated NPSi, Si substrates produced via a 60 min modified MACE process were analyzed on various length scales to obtain information on pore size and interpore spacing by statistical analysis. The commercially purchased stock 5 nm SiO_2–AuNPs particles were found to have a mean gold core diameter of 4 ± 1 nm, whereas the NPSi produced exhibited a resulting mean pore diameter of 6 ± 1 nm and a porosity of 12.5 ± 1% (across three different samples) after MACE (Figure 4A,B). Commercially purchased stock 10 nm SiO_2–AuNPs had a mean diameter of 9 ± 2 nm and were

DOI: 10.1021/acsami.6b01927
ACS Appl. Mater. Interfaces XXXX, XXX, XXX–XXX

shown to produce a mean pore size of 8 ± 3 nm and a porosity of 18.0 ± 3% (across three different samples) in the MACE process (Figure 4C,D). Some of the discrepancy between gold core size and final pore size can be attributed to pore deformation occurring as a result of SEM imaging, likely a result of the high-voltage electron beam effects on the Si. In addition, gold core size and pore size were characterized by TEM and SEM, respectively, which could also contribute to observed disagreement for the 10 nm sample. This approach is necessitated by the extreme difficulty of TEM sample preparation for the post-MACE high-porosity nanoporous silicon. Data from over 1000 pores and 400 particles are used for analysis. Similar results are observed over several micrometers of substrate, and the consistency of etching and coverage is solely limited by the SiO_2−AuNP monolayer quality and coverage. Even if particles are not assembled in ideal monolayers, the SiO_2 spacer ensures a minimum spacing of $\left(\frac{\sqrt{3}}{4}d_t - d_{AuNP}\right)$, where d_t is the particle diameter including the gold core and silica shell and d_{AuNP} is the gold core diameter for up to a trilayer of SiO_2−AuNPs. The deposition of more than a monolayer does however result in a less controllable process by decreasing interpore spacing and increasing porosity unpredictably. As such, the ability to obtain large-area monolayer arrays of SiO_2−AuNPs on the Si surface is crucial for a successful result. Both the sub 10 nm pore sizes and >12% porosities achieved here represent advances over previous ground breaking work by Gaborski et al. that showed NPSi with 10−40 nm pore sizes and 1.44% porosity.[3]

In addition to pore size and interpore spacing, pore depth and aspect ratio are essential metrics for the application of NPSi in membranes and thin films. This was investigated following MACE processing by filling the resulting NPSi pores with aluminum oxide (Al_2O_3) using ALD. ALD was used for the dual purpose of (1) preserving the nanoporous structure and (2) enhancing the image contrast of pores against the Si matrix during cross-sectional milling and SEM imaging, respectively. Cross sections were milled from 60 min MACE samples using focused ion beam milling (FIB) and were then imaged by SEM (Figure 5A,B). The highly conformal nature of the ALD growth and its ability to fill narrow, high aspect ratio structures allows for an accurate representation of the NPSi cross section. Pore filling was verified using energy dispersive X-ray spectroscopy (EDS) analysis within the pore area to show presence of Al and O within bright regions (e.g., Spot 1) and absence of these elements in dark regions (e.g., Spot 2, Figure 5B,C). EDS analysis revealed pore depths of over 500 nm for NPSi produced with both 5 nm (Figure 5A) and 10 nm (Figure 5B) SiO_2−AuNPs, yielding aspect ratios of over 100:1 for the 5 nm NPSi when coupled with the pore size data (Figure 4B). Such aspect ratios have not been previously demonstrated in MACE produced NPSi, with the best recent result being the fabrication of nanotrenches with aspect ratios of 65:1.[56] A possible explanation for this result is the close proximity and consistent spacing of the catalytic AuNPs, which results in uniform hole injection across the entire substrate, yielding excellent anisotropy and producing high aspect ratio pores. Further support for this hypothesis is provided by the observation that 10 nm SiO_2−AuNP catalysts produced shallower nanopores than their 5 nm counterparts after an identical etching time (Figure 5A,B). Close observation of the interpore spacing for the 5 and 10 nm samples reveals more tightly packed pores in the 5 nm case. It is likely that the closer proximity of gold

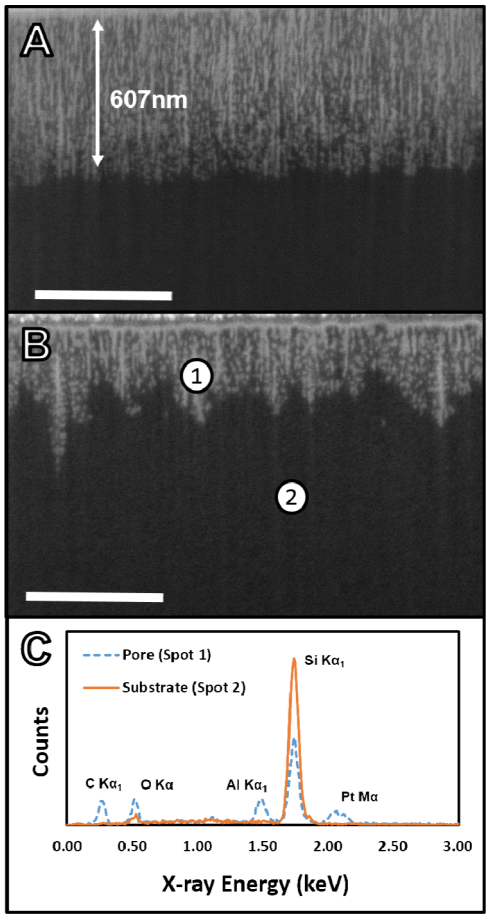

Figure 5. SEM cross-sectional images of FIB milled NPSi produced via the modified MACE process with drop-cast (A) 5 nm and (B) 10 nm SiO_2−AuNPs. Cross sections were analyzed within (Spot 1) and below (Spot 2) the porous area using EDS mapping (C) following the ALD deposition of Al_2O_3 and cross-sectional FIB milling to confirm the presence of Al_2O_3 and by extension elucidate the nanoporous morphology. Scale bars are 500 nm.

particles allowed for more homogeneous hole injection, and therefore a greater etching rate, resulting in deeper pores. To characterize the etching rate over time, cross-sectional samples of NPSi etched with 5 nm SiO_2−AuNP catalysts were imaged after 30 and 60 min (Figure S1). After 30 min of etching, pore depth reached approximately 200 nm, whereas 60 min of etching produced pores approximately 600 nm in depth. The slower rate over the first 30 min of etching may be a result of the time required for the consumption of the silica shell, reorientation of the gold core on the Si surface, and the initiation of etching. Therefore, a more accurate etch rate is obtained by considering the final 30 min of etching, during which time pores are produced in a direction normal to the surface at a rate of approximately 13 nm/min. This rate is not expected to be constant for increased etching times because of the diffusion-limited nature of the etching process.

A final important property of merit for the produced NPSi is chemical and physical stability. Requirements for chemical stability vary drastically with application and as such cannot all be addressed in this work. The demonstrated ability to deposit ultrastable materials such as Al_2O_3 onto the high-aspect ratio pore walls of the produced NPSi (Figure 5) shows that the material can be optimized both for many different applications and for maximum chemical stability. The physical stability of

DOI: 10.1021/acsami.6b01927
ACS Appl. Mater. Interfaces XXXX, XXX, XXX−XXX

the NPSi was investigated by comparing images of a just-produced sample with one stored in air for two months (Figure S2). The morphological similarity between the two samples indicates good structural stability of the material over time.

3. CONCLUSIONS

We have presented a modified highly scalable MACE process that utilizes solution-deposited, self-assembled arrays of SiO_2−AuNPs as catalysts. The developed process improves on the conventional use of noble metal nanoparticle catalysts for the fabrication of NPSi by implementing silica shells as sacrificial spacer layers on AuNPs, which are consumed immediately prior to etching in the MACE solution, allowing for a simple two-step method for the synthesis of NPSi. The ordered, close-packed nature of the SiO_2−AuNPs prior to etching allows for homogeneous injection of holes into the Si substrate, resulting in the highly uniform anisotropic etching of nanopores along crystallographically preferred directions, with little observed lateral etching or clumping of AuNPs. We have demonstrated the ability of the process to produce NPSi with average pore size diameters as low as 6 nm, narrow pore size distributions, porosity of 12.5%, and pore aspect ratio of over 100:1 for substrate areas of many square micrometers. The realization of this novel morphology of Si has the potential to enable its use in numerous applications. Furthermore, the scalability, low cost, and high-throughput nature of the process provide promise for its economic viability in large-scale manufacturing.

■ ASSOCIATED CONTENT

Supporting Information

The Supporting Information is available free of charge on the ACS Publications website at DOI: 10.1021/acsami.6b01927.

SEM images of NPSi. (PDF)

■ AUTHOR INFORMATION

Corresponding Author

*E-mail: jcg@mit.edu.

Funding

We acknowledge the generous financial support of the Abdul Latif Jameel World Water and Food Security Lab at MIT (internal grant) and the MIT Deshpande Center for Technological Innovation (internal grant). B.D.S. receives funding from the Natural Science and Engineering Research Council of Canada (NSERC, Application Number 326004145).

Notes

The authors declare no competing financial interest.

■ ACKNOWLEDGMENTS

This work was performed in part at the Center for Nanoscale Systems (CNS), a member of the National Nanotechnology Infrastructure Network (NNIN), which is supported by the National Science Foundation under NSF award no. ECS-0335765. Special acknowledgement is given to Dr. Andrew Magyar, Adam Graham, and Dr. Jules Gardener for their guidance in materials characterization.

■ REFERENCES

(1) Uhlir, A. J. Electrolytic Shaping of Germanium and Silicon. *Bell Syst. Tech. J.* **1956**, *35*, 333−347.

(2) Striemer, C. C.; Gaborski, T. R.; McGrath, J. L.; Fauchet, P. M. Charge- and Size-Based Separation of Macromolecules Using Ultrathin Silicon Membranes. *Nature* **2007**, *445*, 749−753.

(3) Gaborski, T. R.; Snyder, J. L.; Striemer, C. C.; Fang, D. Z.; Hoffman, M.; Fauchet, P. M.; Mcgrath, J. L. High-Performance Separation of Nanoparticles with Ultrathin Porous Nanocrystalline Silicon Membranes. *ACS Nano* **2010**, *4*, 6973−6981.

(4) Achar, B. H. V; Sengupta, S.; Bhattacharya, E. Fabrication of Ultrathin Silicon Nanoporous Membranes and Their Application in Filtering Industrially Important Biomolecules. *IEEE Trans. Nanotechnol.* **2013**, *12*, 583−588.

(5) Tang, J.; Wang, H.-T.; Lee, D. H.; Fardy, M.; Huo, Z.; Russell, T. P.; Yang, P. Holey Silicon as an Efficient Thermoelectric Material. *Nano Lett.* **2010**, *10*, 4279−4283.

(6) Lee, J.; Lim, J.; Yang, P. Ballistic Phonon Transport in Holey Silicon. *Nano Lett.* **2015**, *15*, 3273−3279.

(7) Li, H.; Yu, Y.; Li, G. Computational Modeling and Analysis of Thermoelectric Properties of Nanoporous Silicon. *J. Appl. Phys.* **2014**, *115*, 124316.

(8) Guo, R.; Huang, B. Thermal Transport in Nanoporous Si: Anisotropy and Junction Effects. *Int. J. Heat Mass Transfer* **2014**, *77*, 131−139.

(9) Yang, C. C.; Li, S. Basic Principles for Rational Design of High-Performance Nanostructured Silicon-Based Thermoelectric Materials. *ChemPhysChem* **2011**, *12*, 3614−3618.

(10) Lee, J.-H.; Galli, G. A.; Grossman, J. C. Nanoporous Si as an Efficient Thermoelectric Material. *Nano Lett.* **2008**, *8*, 3750−3754.

(11) Park, J.-B.; Ham, J.-S.; Shin, M.-S.; Park, H.-K.; Lee, Y.-J.; Lee, S.-M. Synthesis and Electrochemical Characterization of Anode Material with Titanium−Silicon Alloy Solid Core/Nanoporous Silicon Shell Structures for Lithium Rechargeable Batteries. *J. Power Sources* **2015**, *299*, 537−543.

(12) Kim, H.; Han, B.; Choo, J.; Cho, J. Three-Dimensional Porous Silicon Particles for Use in High-Performance Lithium Secondary Batteries. *Angew. Chem., Int. Ed.* **2008**, *47*, 10151−10154.

(13) Bang, B. M.; Kim, H.; Lee, J.-P.; Cho, J.; Park, S. Mass Production of Uniform-Sized Nanoporous Silicon Nanowire Anodes via Block Copolymer Lithography. *Energy Environ. Sci.* **2011**, *4*, 3395−3399.

(14) Yu, Y.; Gu, L.; Zhu, C.; Tsukimoto, S.; van Aken, P. A.; Maier, J. Reversible Storage of Lithium in Silver-Coated Three-Dimensional Macroporous Silicon. *Adv. Mater.* **2010**, *22*, 2247−2250.

(15) Klankowski, S. A.; Pandey, G. P.; Malek, G. A.; Wu, J.; Rojeski, R. A.; Li, J. A Novel High-Power Battery-Pseudocapacitor Hybrid Based on Fast Lithium Reactions in Silicon Anode and Titanium Dioxide Cathode Coated on Vertically Aligned Carbon Nanofibers. *Electrochim. Acta* **2015**, *178*, 797−805.

(16) Omampuliyur, R. S.; Bhuiyan, M.; Han, Z.; Jing, Z.; Li, L.; Fitzgerald, E. A.; Thompson, C. V.; Choi, W. K. Nanostructured Thin Film Silicon Anodes for Li-Ion Microbatteries. *J. Nanosci. Nanotechnol.* **2015**, *15*, 4926−4933.

(17) Ivanov, S.; Vlaic, C.; Du, S.; Wang, D.; Schaaf, P.; Bund, A. Electrochemical Performance of Nanoporous Si as Anode for Lithium Ion Batteries in Alkyl Carbonate and Ionic Liquid-Based Electrolytes. *J. Appl. Electrochem.* **2014**, *44*, 159−168.

(18) Hsu, C.-H.; Wu, J.-R.; Lu, Y.-T.; Flood, D. J.; Barron, A. R.; Chen, L.-C. Fabrication and Characteristics of Black Silicon for Solar Cell Applications: An Overview. *Mater. Sci. Semicond. Process.* **2014**, *25*, 2−17.

(19) Lu, Y.-T.; Barron, A. R. Nanopore-Type Black Silicon Anti-Reflection Layers Fabricated by a One-Step Silver-Assisted Chemical Etching. *Phys. Chem. Chem. Phys.* **2013**, *15*, 9862−9870.

(20) Lu, Y.-T.; Barron, A. R. Anti-Reflection Layers Fabricated by a One-Step Copper-Assisted Chemical Etching with Inverted Pyramidal Structures Intermediate Between Texturing and Nanopore-Type Black Silicon. *J. Mater. Chem. A* **2014**, *2*, 12043−12052.

(21) Huang, M.-J.; Yang, C.-R.; Chiou, Y.-C.; Lee, R.-T. Fabrication of Nanoporous Antireflection Surfaces on Silicon. *Sol. Energy Mater. Sol. Cells* **2008**, *92*, 1352−1357.

(22) Li, X. Metal Assisted Chemical Etching for High Aspect Ratio Nanostructures: A Review of Characteristics and Applications in Photovoltaics. *Curr. Opin. Solid State Mater. Sci.* **2012**, *16*, 71−81.

DOI: 10.1021/acsami.6b01927
ACS Appl. Mater. Interfaces XXXX, XXX, XXX−XXX

(23) Chong, T. K.; Bullock, J.; White, T. P.; Berry, M.; Weber, K. J. Nanoporous Silicon Produced by Metal-Assisted Etching: A Detailed Investigation of Optical and Contact Properties for Solar Cells. *IEEE J. Photovolt.* **2015**, *5*, 538−544.
(24) Shi, J.; Xu, F.; Ma, Z.; Zhou, P.; Zheng, L.; Yang, J.; Chen, D.; Jiang, Z. Nanoporous Black Multi-Crystalline Silicon Solar Cells: Realization of Low Reflectance and Explanation of High Recombination Loss. *Mater. Sci. Semicond. Process.* **2013**, *16*, 441−448.
(25) Toor, F.; Branz, H. M.; Page, M. R.; Jones, K. M.; Yuan, H.-C. Multi-Scale Surface Texture to Improve Blue Response of Nanoporous Black Silicon Solar Cells. *Appl. Phys. Lett.* **2011**, *99*, 103501.
(26) Yuan, H.-C.; Yost, V. E.; Page, M. R.; Stradins, P.; Meier, D. L.; Branz, H. M. Efficient Black Silicon Solar Cell With a Density-Graded Nanoporous Surface: Optical Properties, Performance Limitations, and Design Rules. *Appl. Phys. Lett.* **2009**, *95*, 123501.
(27) Oh, J.; Deutsch, T. G.; Yuan, H.-C.; Branz, H. M. Nanoporous Black Silicon Photocathode for H_2 Production by Photoelectrochemical Water Splitting. *Energy Environ. Sci.* **2011**, *4*, 1690−1694.
(28) Liu, P.; Yang, F.; Wang, W.; Luo, K.; Wang, Y.; Zhang, D. Hard Mask Free DRIE of Crystalline Si Nanobarrel with 6.7nm Wall Thickness and 50:1 Aspect Ratio. *IEEE Int. Conf. Micro Electro Mech. Syst., 28th* **2015**, 77−80.
(29) Liu, Z.; Gu, X.; Hwu, J.; Sassolini, S.; Olynick, D. L. Low-Temperature Plasma Etching of High Aspect-Ratio Densely Packed 15 to sub-10 nm Silicon Features Derived from PS-PDMS Block Copolymer Patterns. *Nanotechnology* **2014**, *25*, 285301.
(30) Li, X.; Bohn, P. W. Metal-Assisted Chemical Etching in HF/H_2O_2 Produces Porous Silicon. *Appl. Phys. Lett.* **2000**, *77*, 2572−2574.
(31) Huang, Z.; Geyer, N.; Werner, P.; de Boor, J.; Gösele, U. Metal-Assisted Chemical Etching of Silicon: a Review. *Adv. Mater.* **2011**, *23*, 285−308.
(32) Chartier, C.; Bastide, S.; Lévy-Clément, C. Metal-Assisted Chemical Etching of Silicon in HF−H_2O_2. *Electrochim. Acta* **2008**, *53*, 5509−5516.
(33) Harada, Y.; Li, X.; Bohn, P. W.; Nuzzo, R. G. Catalytic Amplification of the Soft Lithographic Patterning of Si. Nonelectrochemical Orthogonal Fabrication of Photoluminescent Porous Si Pixel Arrays. *J. Am. Chem. Soc.* **2001**, *123*, 8709−8717.
(34) Lai, C. Q.; Cheng, H.; Choi, W. K.; Thompson, C. V. Mechanics of Catalyst Motion During Metal Assisted Chemical Etching of Silicon. *J. Phys. Chem. C* **2013**, *117*, 20802.
(35) Chern, W.; Hsu, K.; Chun, I. S.; de Azeredo, B. P.; Ahmed, N.; Kim, K.-H.; Zuo, J.; Fang, N.; Ferreira, P.; Li, X. Nonlithographic Patterning and Metal-Assisted Chemical Etching for Manufacturing of Tunable Light-Emitting Silicon Nanowire Arrays. *Nano Lett.* **2010**, *10*, 1582−1588.
(36) Liu, Y.; Sun, W.; Jiang, Y.; Zhao, X.-Z. Fabrication of Bifacial Wafer-Scale Silicon Nanowire Arrays with Ultra-High Aspect Ratio Through Controllable Metal-Assisted Chemical Etching. *Mater. Lett.* **2015**, *139*, 437−442.
(37) Chang, S.-W.; Chuang, V. P.; Boles, S. T.; Ross, C. A.; Thompson, C. V. Densely Packed Arrays of Ultra-High-Aspect-Ratio Silicon Nanowires Fabricated Using Block-Copolymer Lithography and Metal-Assisted Etching. *Adv. Funct. Mater.* **2009**, *19*, 2495−2500.
(38) Huang, Z.; Zhang, X.; Reiche, M.; Liu, L.; Lee, W.; Shimizu, T.; Senz, S.; Gösele, U. Extended Arrays of Vertically Aligned Sub-10 nm Diameter [100] Si Nanowires by Metal-Assisted Chemical Etching. *Nano Lett.* **2008**, *8*, 3046−3051.
(39) Chen, H.; Wang, H.; Zhang, X.-H.; Lee, C.-S.; Lee, S.-T. Wafer-Scale Synthesis of Single-Crystal Zigzag Silicon Nanowire Arrays with Controlled Turning Angles. *Nano Lett.* **2010**, *10*, 864−868.
(40) Smith, Z. R.; Smith, R. L.; Collins, S. D. Mechanism of Nanowire Formation in Metal Assisted Chemical Etching. *Electrochim. Acta* **2013**, *92*, 139−147.
(41) Benoit-Moez, C.; Bastide, S.; Levy-Clement, C. Formation of Si Nanowire Arrays by Metal-Assisted Chemical Etching. *ECS Trans.* **2008**, *16*, 245−252.
(42) Peng, K.; Lu, A.; Zhang, R.; Lee, S.-T. Motility of Metal Nanoparticles in Silicon and Induced Anisotropic Silicon Etching. *Adv. Funct. Mater.* **2008**, *18*, 3026−3035.
(43) Güder, F.; Yang, Y.; Küçükbayrak, U. M.; Zacharias, M. Tracing the Migration History of Metal Catalysts in Metal-Assisted Chemically. *ACS Nano* **2013**, *7*, 1583−1590.
(44) Scheeler, S. P.; Ullrich, S.; Kudera, S.; Pacholski, C. Fabrication of Porous Silicon by Metal-Assisted Etching Using Highly Ordered Gold Nanoparticle Arrays. *Nanoscale Res. Lett.* **2012**, *7*, 450.
(45) Zhu, J.; Bart-Smith, H.; Begley, M. R.; Zangari, G.; Reed, M. L. Formation of Silicon Nanoporous Structures Induced by Colloidal Gold Nanoparticles in HF/H_2O_2 Solutions. *Chem. Mater.* **2009**, *21*, 2721−2726.
(46) Lee, C.-L.; Tsujino, K.; Kanda, Y.; Ikeda, S.; Matsumura, M. Pore Formation in Silicon by Wet Etching Using Micrometre-Sized Metal Particles as Catalysts. *J. Mater. Chem.* **2008**, *18*, 1015−1020.
(47) Yoon, S.-S.; Khang, D.-Y. Direct Visualization of Etching Trajectories in Metal-Assisted Chemical Etching of Si by the Chemical Oxidation of Porous Sidewalls. *Langmuir* **2015**, *31*, 10549−10554.
(48) Tsujino, K.; Matsumura, M. Morphology of Nanoholes Formed in Silicon by Wet Etching in Solutions Containing HF and H_2O_2 at Different Concentrations Using Silver Nanoparticles as Catalysts. *Electrochim. Acta* **2007**, *53*, 28−34.
(49) Asoh, H.; Fujihara, K.; Ono, S. Sub-100-nm Ordered Silicon Hole Arrays by Metal-Assisted Chemical Etching. *Nanoscale Res. Lett.* **2013**, *8*, 410.
(50) Chang, C.; Sakdinawat, A. Ultra-High Aspect Ratio High-Resolution Nanofabrication for Hard X-ray Diffractive Optics. *Nat. Commun.* **2014**, *5*, 4243.
(51) Perrey, C. R.; Carter, C. B. Insights into Nanoparticle Formation Mechanisms. *J. Mater. Sci.* **2006**, *41*, 2711−2722.
(52) Min, Y.; Akbulut, M.; Kristiansen, K.; Golan, Y.; Israelachvili, J. The Role of Interparticle and External Forces in Nanoparticle Assembly. *Nat. Mater.* **2008**, *7*, 527−538.
(53) Vanderkooy, A.; Chen, Y.; Gonzaga, F.; Brook, M. A. Silica Shell/Gold Core Nanoparticles: Correlating Shell Thickness with the Plasmonic Red Shift upon Aggregation. *ACS Appl. Mater. Interfaces* **2011**, *3*, 3942−3947.
(54) Mine, E.; Yamada, A.; Kobayashi, Y.; Konno, M.; Liz-Marzán, L. M. Direct Coating of Gold Nanoparticles with Silica by a Seeded Polymerization Technique. *J. Colloid Interface Sci.* **2003**, *264*, 385−390.
(55) Wu, Y.; Zhang, C.; Yuan, Y.; Wang, Z.; Shao, W.; Wang, H.; Xu, X. Fabrication of Wafer-Size Monolayer Close-Packed Colloidal Crystals via Slope Self-Assembly and Thermal Treatment. *Langmuir* **2013**, *29*, 14017−14023.
(56) Booker, K.; Brauers, M.; Crisp, E.; Rahman, S.; Weber, K.; Stocks, M.; Blakers, A. Metal-Assisted Chemical Etching for Very High Aspect Ratio Grooves in n-Type Silicon Wafers. *J. Micromech. Microeng.* **2014**, *24*, 125026.

DOI: 10.1021/acsami.6b01927
ACS Appl. Mater. Interfaces XXXX, XXX, XXX−XXX